IEEE Access
Multidisciplinary | Rapid Review | Open Access Journal

Date of publication xxxx 00, 0000, date of current version xxxx 00, 0000.

Digital Object Identifier 10.1109/ACCESS.2017.DOI

Signal Characterization and Achievable Transmission Rate of VLC Under Receiver Nonlinearity

XIAONA LIU[1], CHEN GONG[2], DIFAN ZOU[3], ZUNAIRA BABAR[4], ZHENGYUAN XU[2] AND LAJOS HANZO,[4] (Fellow, IEEE)

[1]The Future Network of Intelligence Institute, Chinese University of Hongkong, Shenzhen, Guangdong 518172, China
[2]Department of Electrical Engineering and Information Science, University of Science and Technology of China, Hefei, Anhui 230027, China
[3]Department of Computer Science, University of Los Angeles, California, CA 90095, USA
[4]School of Electronics and Computer Science, University of Southampton, Southampton SO17 1BJ, U.K.

Corresponding author: Chen Gong (e-mail: cgong821@ustc.edu.cn).

This work was collaboratively done by Key Laboratory of Wireless-Optical Communications, Chinese Academy of Sciences, School of Information Science and Technology, University of Science and Technology of China, China and Wireless Group of School of Electronics and Computer Science, University of Southampton, UK. This work was supported by Key Program of National Natural Science Foundation of China (Grant No. 61631018), Key Research Program of Frontier Sciences of CAS (Grant No. QYZDYSSW- JSC003).

ABSTRACT Strong ambient light and the resultant photoelectric conversion saturation of an avalanche photo diode (APD) may signficantly deteriorate the received signal in visible light communication (VLC) systems. Hence, in this paper we characterize the signal received from an APD under strong ambient light based on our experimental data. To illustrate the phenomenon of APD saturation, we investigate the transmission rate and analyze the link budget. In order to achieve dimming control, we then conceive a unary-coded VLC system for maintaining the user-defined dimming level. We calculate both the upper and lower bounds of the achievable transmission rate of the unary-coded VLC system.

INDEX TERMS Visible light communication, photoelectric conversion, saturation.

I. INTRODUCTION

The past decade has witnessed rapid developments in the realms of visible light communication (VLC) [1]. The commonly used transmission source of VLC is the ubiquitous light-emitting diode (LED), which is gaining popularity due to its low power consumption and long life time. It is anticipated that the LED-based lighting infrastructure will inevitably replace the conventional lighting infrastructure. This has in turn given rise to a new research horizon focusing on VLC systems, since LEDs efficiently serve the dual purposes of lighting and communication. In this context, wireless networking relying on VLC, which is referred to as Light Fidelity (LiFi), was introduced in 2011 [2] and it has been included in IEEE standards [3]. There have been significant advances on LiFi during the past ten years. Consequently, the link data rates have increased three orders of magnitude from 10 Mbps in the year 2006 to 10 Gbps in 2016 [4], [5]. It is worth mentioning that even with a single LED, a VLC system can achieve a data rate exceeding 3 Gb/s [4]. Owing to the ubiquitous solar background radiation, VLC signals cannot be transmitted over a long distance during day time. The limited modulation bandwidth of the commercial LED devices is another disadvantage of VLC. Moreover, the line-of-sight (LOS) VLC links may become blocked, which results in weak received signal power. Hence, the signal characterization under a large dynamic range of received power, including the strong and weak power regime, has to be further investigated.

For the sake of satisfying the primary lighting constraints during communications, joint dimming and communication system designs have been conceived for OFDM transmission [6], [7] and Pulse-Position Modulation (PPM) aided transmission [8], [9], respectively. The system performance under various lighting constraints has been investigated in [10]–[13]. A system optimization framework for VLC under lighting constraints has been proposed in [14]. Moreover, a beamforming aided visible light communication system has been studied in [15]–[17]. It is noteworthy that in [16], the joint beamforming and direct-current (DC) bias design problem has been investigated considering signal-dependent shot noise.

Strong ambient light can shift the incident optical power

to the saturation regime, which can lead to extremely low SNR in the electric signal detector. The authors of [18], [19] considered this extreme scenario for VLC communication and proposed to study light-off communication and dark light communications, respectively. Another solution proposed by the authors of [20] advocated using high pass filtering for mitigating the background light which may be viewed as a near-constant light-level. This measure has indeed succeeded in mitigating the deleterious impairments of strong background light, but unfortunately it has increased the amount of shot-noise which is proportional to the bandwidth. In order to cope with this undesired effect, the concept of adaptive bandwidth was introduced, which was controlled by the amount of background light. As a further a benefit, this system was capable of operating even in outdoor scenarios.

Most existing contributions on VLC assume a linear relationship between the transmitted optical power and the received electric signal. However, this assumption heavily relies on the premise that the photoelectric conversion is operating in the linear domain, which may not hold for the entire range of incident light power. For example, the detector may become saturated in strong ambient light, so that the output signal variations with respect to the transmitted power become negligible, leading to a low signal-to-noise ratio (SNR). Hence, the VLC system design should incorporate these effects, in order to cater for a wider range of ambient light power. For the sake of achieving this objective, in this paper we investigate the channel characteristics and link budget for a wide ambient light power range assuming realistic photoelectric conversion.

Recall that VLC systems serve the dual purposes of illumination and communication. For the sake of flawlessly supporting the illumination function, we also have to provide flicker-mitigation and dimming control. Dimming control is particularly important for indoor applications, where a user may want to maintain a desired lighting ambiance. In [21], the authors compared several dimming control schemes, namely inverse source coding, multi-pulse position modulation (MPPM) and unary-coded dimming control. The unary code aided dimming scheme was shown to outperform its conterparts for an ON-OFF keying (OOK) modulated VLC system. It was also demonstrated that the unary code is capable of providing flicker-free illumination [21].

Against this background, in this paper we have designed and investigated a unary coded VLC system operating under strong ambient light. Our novel contributions are:

1) We design and conduct experiments to characterize the signal statistics of the nonlinear photoelectric conversion outputs, especially in the saturation region.
2) We investigate the achievable transmission rate of the system and analyze the link budget in a realistic transmission scenario.
3) We calculate the upper and lower bounds on the achievable transmission rate for the unary-coded VLC system.
4) Finally, we adopt trellis-based Viterbi decoding for detecting the variable length unary coded signals. We demonstrate that the proposed Viterbi decoder outperforms the maximum likelihood ratio (MLR) based decoder in terms of the bit error ratio (BER).

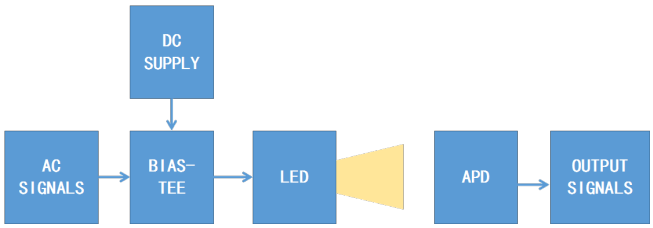

FIGURE 1. The communication system model with unary-coded dimming control.

II. SYSTEM MODEL AND SIGNAL CHARACTERIZATION

In this section, we characterize the nonlinear photoelectric conversion of the avalanche photo diode (APD) receiver. Recall that due to the illuminance functionality of VLC, joint dimming and communication optimization has to be performed. Typically, the DC component is used for illuminance, while the alternate current (AC) component is used for communication. Due to the APD saturation effect arising from strong ambient intensity, the peak-to-peak voltage of the APD output signal may decrease for high DC voltages. In this section, we aim for characterizing this phenomenon based on practical experimental measurements. The system is shown in Figure 1. In the proposed system, we adopt unary dimming control before the LED driving circuit. Again, the AC component supports communications, while the DC component drives the LED. Both the AC and DC components drive the LED through the Bias-Tee. A high DC component results in strong ambient light. The dimming level γ can be designed by the unary-coding. At the receiver side, an APD is used for detecting the signals under strong ambient light.

We carried out an experiment to obtain the key system parameters affecting the saturation. The transmitter and receiver were put into a sealed box without ambient radiation from outside. At the transmitter side, we varied the DC component V_{DC} and AC component Vpp_{in} to create different DC and AC components of the light power at the receiver surface. At the receiver side, we measured the APD output signal after the photoelectric conversion and recorded both the peak-to-peak voltage as well as the noise variance of the output signal.

We used the Rigol DG5252 arbitrary waveform generator (AWG) to generate random data and to drive the LED arrays with on-off keying (OOK) modulation, where the power was supplied via a bias-tee. At the receiver side, a Hamamatsu C12702 model APD with DC filtering was employed to detect the optical signals. An OPHIR Photonics Nova II P/N 7Z01550 optical power meter was employed to measure the received optical power and to calculate the power on the detector's surface, based on the ratio of the area of the power meter over the area of the detector. Furthermore, an Agilent MSOX6004A oscilloscope was used to capture and save the APD's output data for further offline processing in

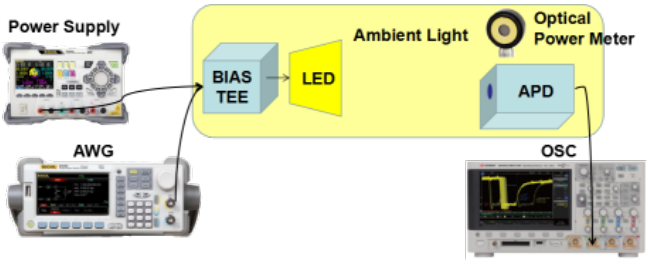

FIGURE 2. The experimental system diagram.

the computer. The experimental system is shown in Figure 2. We set the low voltage of the OOK signal to 0V and varied the high voltage V_{AC} from 0V to 1V with a step size of 0.02V. To drive the LED and to generate different ambient light intensities, the DC voltage V_{DC} on the bias-tee varied from 23V to 26V with a step size of 0.02V. Note that a high DC voltage can create strong ambient light.

Since the LED transmits OOK signals, we can obtain the mean voltages and variances of the OOK symbols one and zero from the output data of the Agilent MSOX6004A oscilloscope. The mean and variance of the symbol one are shown in Figures 3 and 4, respectively, against the DC component and AC component of the driving signal, where the APD has removed the DC component. Observe from Figure 3 that the average output signal amplitude changes with both the DC and AC components of the input signal. Similar trends can be observed from Figure 4 for the signal variance with respect to the DC and AC components, based on a sufficiently high number of transmitted frames.

We also plot the optical power variation with the DC input voltage in Figure 5. Observe that given the AC component, the mean and variance of symbol one first increase and then decrease with the DC voltage. This is due to the associated photoelectric conversion characteristics, where the peak-to-peak output voltage first increases upon increasing the incident light power, and then decreases due to the saturation effect. Explicitly, higher DC components result in stronger ambient light. Consequently, the APD is driven into its saturation mode. Thereafter, any further increase of the DC voltage leads to the reduction of the peak-to-peak output voltage. The peak value of the mean and variance is observed at a DC voltage of 23.5V. Please note that the mean of the symbol zero is analogous to that of symbol one, but has a negative polarity. Similarly, the variance of the OOK symbol zero has a similar shape as that of symbol one, i.e. it first increases with the DC voltage and then decreases with it. However, the variance of symbol zero is lower than that of symbol one, due to the shot noise, which increases with the incident power. The variance corresponding to the DC component voltages is plotted in Figure 6, which reaches its peak value at the DC voltage of 23.5V and then decreases as the DC voltage grows.

Figures 3,4,5 and 6 are plotted directly based on the experimental data. From the above signal characterization,

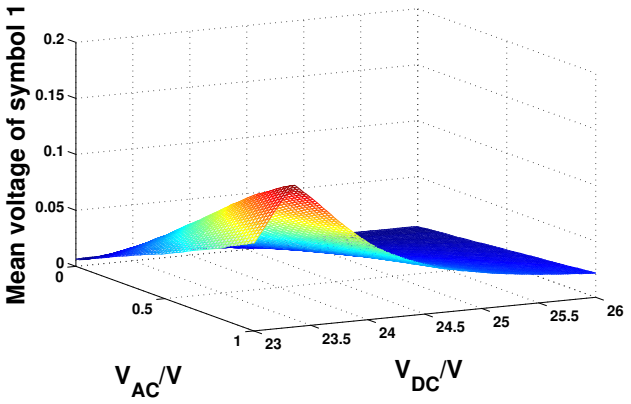

FIGURE 3. Mean of APD output signals corresponding to symbol one.

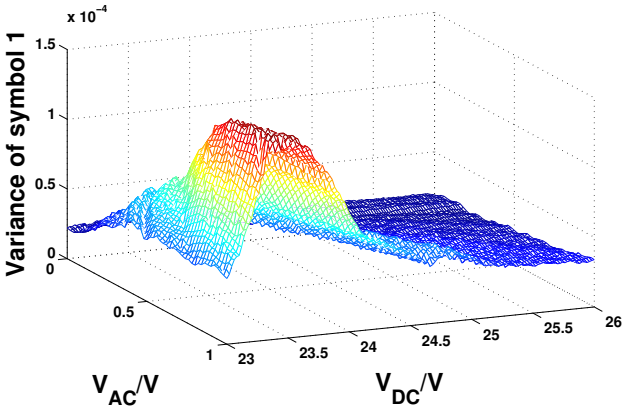

FIGURE 4. Variance of APD output signals corresponding to symbol one.

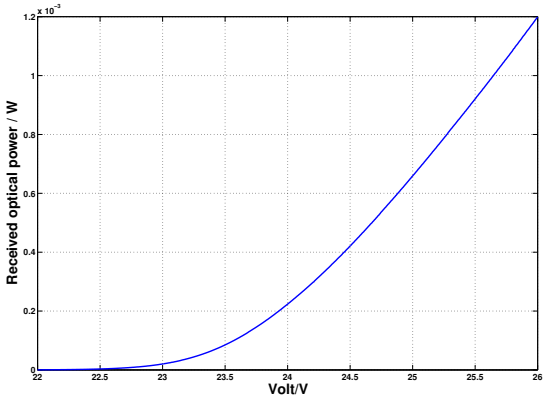

FIGURE 5. The optical power with respect to the input DC voltages at the APD receiver side.

we conclude that the output signals for the OOK symbols one and zero satisfy two different Gaussian distributions, with opposite mean values and different variances. More specifically, the output signals Y_1 and Y_0 for the symbols one and zero, respectively, may be modeled using the following

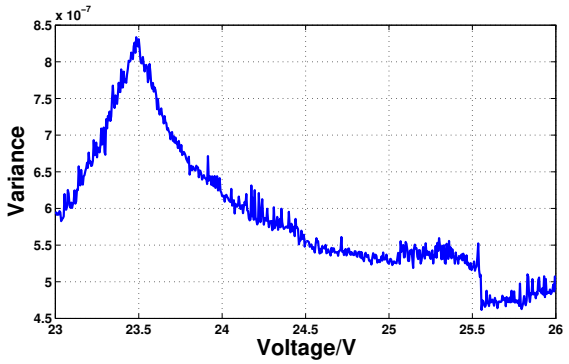

FIGURE 6. The variance with the input DC voltages at the APD receiver side.

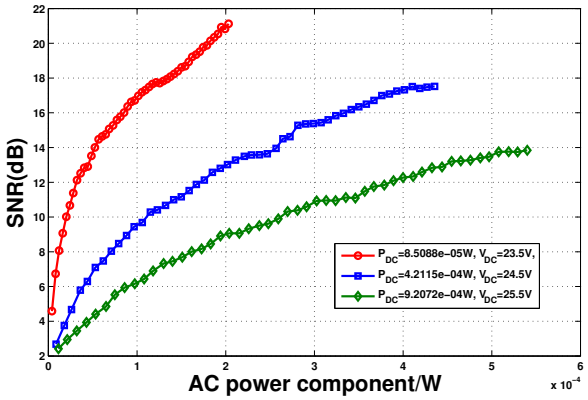

FIGURE 7. The SNR of OOK signal at the APD receiver side.

Gaussian distributions,

$$Y_0 \sim \mathcal{N}(-\mu, \sigma_0^2), \quad (1)$$
$$Y_1 \sim \mathcal{N}(\mu, \sigma_1^2), \quad (2)$$

where μ denotes the mean value, while σ_0^2 and σ_1^2 denote the variances of the OOK symbols zero and one, respectively. Furthermore, the mean voltage of Figure 3 characterizes the received signal intensities. It can be observed that both the signal intensities and noise variances grow, as the AC component amplitude increases. The signal and noise components will reach the maximum level and then decrease with the DC component. Thus we also plot the signal to noise ratio (SNR) at the APD side in Figure 7. It is seen that for a lower DC power component, the SNR is higher for a fixed AC power component.

III. TRANSMISSION RATE AND LINK BUDGET UNDER AMBIENT LIGHT

In Section II, we observe that strong ambient light saturates the APD. Hence, it is important to quantify the transmission and link budget under strong ambient light. We aim for estimating the achievable transmission rate based on the signal component and noise component analysis.

A. ACHIEVABLE TRANSMISSION RATE

In this section, we derive the achievable transmission rate under strong ambient light, based on the experimental statistics of the photoelectric conversion outputs discussed in Section II. Let X denote the modulated signal and Y denote the photoelectric conversion output signal. Then, the achievable transmission rate is given by

$$I(X;Y) = H(Y) - H(Y|X), \quad (3)$$

where the entropy and conditional entropy is given as follows,

$$H(Y) = -\int_Y P(Y)\log(P(Y)dY, \quad (4)$$
$$P(Y) = P(X=0)P(Y|X=0) + P(X=1)P(Y|X=1), \quad (5)$$
$$H(Y|X) = P(X=1)H(Y|X=1) + P(X=0)H(Y|X=0). \quad (6)$$

Recall from Eq.(1) and Eq.(2) that Y satisfies a mixed Gaussian distribution having two normal distributions of different standard deviations. Let us assume that the input bits are equiprobable, i.e., $P(X=0) = P(X=1) = 1/2$. Thus the conditional entropy $H(Y|X)$ can be readily calculated based on the normal distribution properties $H(Y|X) = \frac{1}{4}\log(2\pi e\sigma_0^2) + \frac{1}{4}\log(2\pi e\sigma_1^2)$. Consequently, the mutual information $I(X;Y)$, which characterizes the achievable transmission rate, can be expressed as follows:

$$I(\mathbf{X};\mathbf{Y}) = H(\mathbf{Y}) - \frac{1}{4}\log(2\pi e\sigma_0^2) - \frac{1}{4}\log(2\pi e\sigma_1^2). \quad (7)$$

Furthermore, $P(Y) = P(X=0)P(Y|X=0) + P(X=1)P(Y|X=1)$ in Eq(3) obeys a mixed Gaussian distribution. We resort to Monte-Carlo simulation to obtain a numerical solution for the entropy $H(Y)$ based on the statistics obtained from the experimental results.

In Figure 8, we plot the achievable transmission rate under different combinations of DC and AC inputs. It may be observed in Figure 8 that for a given DC voltage, the achievable transmission rate approaches one upon increasing the AC power. Furthermore, the transmission rate decreases upon increasing the DC voltage. However, we may further observe in Figure 9 that when the AC power is very low, the transmission rate increases upon increasing the DC power until reaching a maximum value. Thereafter, the transmission rate decreases upon increasing the DC power.

B. LINK BUDGET

In a real communication system, the incident light power corresponding to the OOK symbols one and zero can be calculated using the LED light power, as well as the transmitter-receiver link gain according to the transceiver geometry. Hence, in this section we provide our link budget analysis. The transmission rate expression of Section III-A (Equation (7)) is considered for analyzing the impact of the saturation on the achievable transmission rate at various transmission distances.

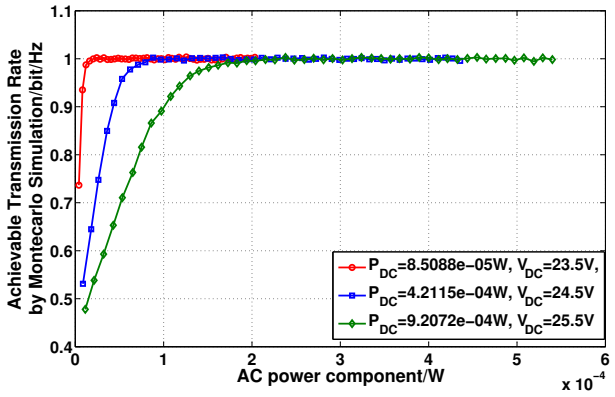

FIGURE 8. The achievable transmission rate from Monte-Carlo simulation with respect to the AC component given different DC components.

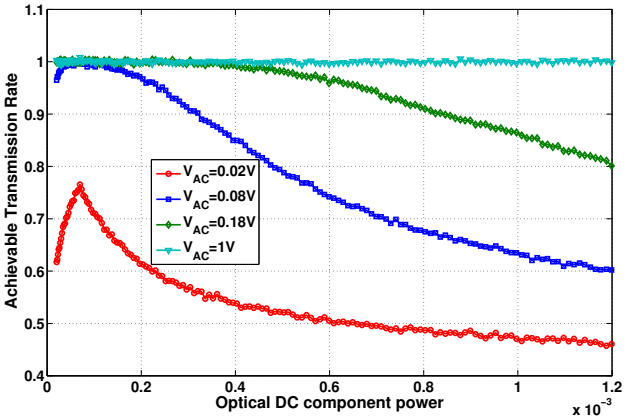

FIGURE 9. The achievable transmission rate from Monte-Carlo simulation

Let us assume that the LED is a Lambertian source. Given the negligible reflection from the walls, only the line of sight (LOS) link dominates. For a receiver located at a distance d and angle ϕ with respect to the LED, the link gain is given by

$$H_{LOS} = \begin{cases} \dfrac{A_r(m_1+1)}{2\pi d^2}\cos^{m_1}(\phi)\cos(\psi), & 0 \le \psi \le \Psi_c; \\ 0, & \text{otherwise}; \end{cases} \tag{8}$$

where ψ is the angle of incidence at the receiver, Φ_c is the FOV of the receiver and m_1 is the order of Lambertian emission related to the LED semi-angle at half-power $\Phi_{1/2}$, formulated as follows:

$$m_1 = \frac{-\ln 2}{\ln(\cos\Phi_{1/2})}. \tag{9}$$

Let us assume that the transmitter's LED power varies between P_{tH} and P_{tL}. Consequently, the power at the receiver surface will vary between P_{rH} and P_{rL}, where P_{rH} and P_{rL} are related to P_{tH} and P_{tL} as follows:

$$P_{rH} = H_{LOS}P_{tH}, \;\; P_{rL} = H_{LOS}P_{tL}. \tag{10}$$

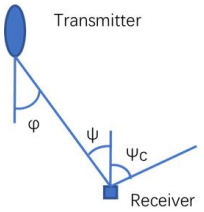

FIGURE 10. Geometry model of VLC.

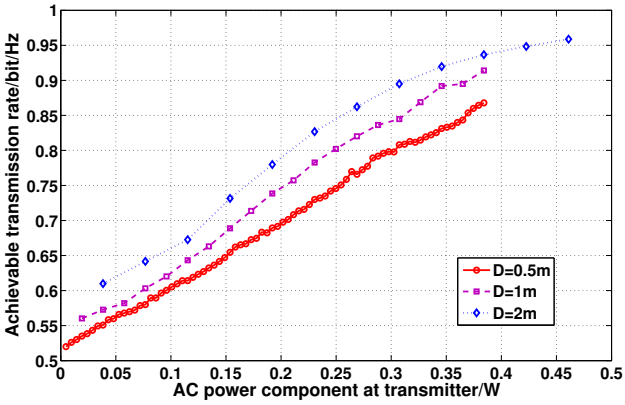

FIGURE 11. The achievable transmission rate under different transmission distances for the DC component of 5W.

The total light power at the receiver will also include the ambient light power. Hence, the light power at the receiver surface will vary between $P_{rH}+P_a$ and $P_{rL}+P_a$, where P_a denotes the ambient light power.

According to the experimental data shown in Figure 3 and Figure 4, we can now carry out the link budget analysis. Figure 11 presents the achievable transmission rate upon varying the AC power and the transmission distances, when the DC power is fixed to $5W$. It may be observed in Figure 11 that the achievable transmission rate decreases upon reducing the transmission distance. This is due to the saturation effect of the receiver-side photoelectric conversion.

Figure 12 shows the achievable transmission rate against the AC power for DC power components of 1W, 3W, and 5W, at the transmission distance of one meter. It is seen that for a fixed AC power, the achievable transmission rate decreases upon increasing the DC component. This is because a stronger optical power moves the operating point of the photoelectric conversion to the saturation region. Furthermore, the transmission rate increases upon increasing the AC power until it approaches one, which is the maximum achievable rate of OOK modulation.

It can be readily seen from the above results that the saturation of the APD degrades the output signals, which also decreases the transmission rate. Thus it is important to consider the saturation as part of the VLC system optimization.

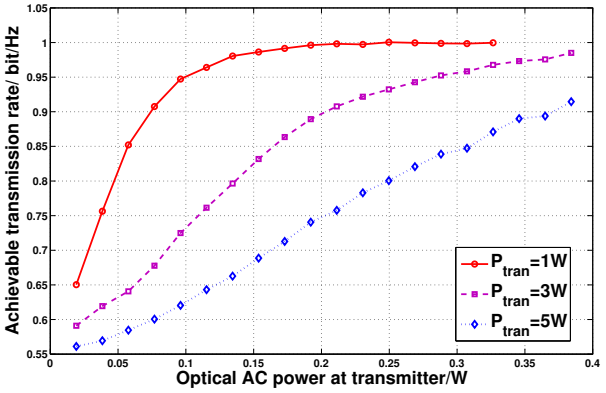

FIGURE 12. The achievable transmission rate under different DC power components for transmission distance of one meter.

IV. TRANSMISSION RATE WITH UNARY-CODED DIMMING CONTROL

In practical scenarios, a user may want to adjust the dimming level according to the requirements, such as mood/ambience. Here, we invoke unary-coded dimming control for adjusting the illuminance of the LED transmitter. Again, we have chosen unary-coded dimming control because it was demonstrated in [21] that unary codes provide attractive throughput gains over their counterparts, while also ensuring a flicker-free dimming level. Unary codes belong to the family of variable length source codes. They map each symbol i onto an i-bit codeword, which has (i-1) 1's followed by a zero (or equivalently $(i-1)$0's followed by a one). For example, the 4-level unary coding scheme maps symbols $\{1,\ 2,\ 3,\ 4\}$ onto $\{0,\ 10,\ 110,\ 1110\}$. This results in a throughput of 0.8 bit per symbol and a dimming level of 0.6, given that the codewords have a uniform distribution. The detailed unary-coded mapping is provided in Table I of [21].

A. UPPER BOUND

In this section, we derive the upper bound of the achievable rate of a unary coded transmission, based on a distribution $Q(Y)$ to compute the Kullback-Leibler (KL) distance of $P(Y|S)$ and $Q(Y)$. Explicitly, for two distributions $p(x)$ and $q(x)$, the KL distance is given by

$$D[p(x)||q(x)] = \int p(x) \ln \frac{p(x)}{q(x)} dx, \tag{11}$$

for continuous distributions; and by

$$D[p(x)||q(x)] = \sum_x p(x) \ln \frac{p(x)}{q(x)}, \tag{12}$$

for discrete distributions. It can be shown that $D[p(x)||q(x)] \geq 0$, and the equality is achieved if and only if $p(x) = q(x)$ for all x.

We propose to derive Q as the bit-wise output distribution of Y, since in a 4-level unary-coded stream the occurance probability of bit 0 is 40% and of bit 1 is 60%, independently of each other. Note that $I(X;Y)$ is the bit level mutual information and $I(S;Y)$ is the symbol level mutual information. Let us assume that L is the average code length. Then for unary 4 coding we have $L = 2.5$. Then, we arrive at

$$\begin{aligned} I(X;Y) &= I(S;Y)/L; && (13)\\ I(S;Y) &\leq H(S); && (14)\\ I(S;Y) &= D(P_{Y|S}||Q|S) - D(P_Y||Q) && (15)\\ &\leq \sum_S D(P_{Y|S}||Q|S), && (16) \end{aligned}$$

where Equation (15) can be derived as follows, with S representing the input symbols, and Q the bit-wise distribution, which can be appropriately designed. Then we arrive at:

$$\begin{aligned} I(S;Y) &= \sum_{\{S,Y\}} \left\{ P(S,Y) \log \frac{P(S,Y)}{P(S)P(Y)} \right\} \\ &= \sum_{\{S,Y\}} \left\{ P(S,Y) \log \frac{P(Y|S)}{P(Y)} \right\} \\ &= \sum_{\{S,Y\}} \left\{ P(Y|S)P(S) \log \frac{P(S|Y)}{Q} \right\} \\ &\quad - \sum_{\{S,Y\}} \left\{ P(Y|S)P(S) \log \frac{P(Y)}{Q} \right\} \\ &= \sum_S [P(S)D(P(Y|S)||Q)] - \sum_Y \left\{ P(Y) \log \frac{P(Y)}{Q} \right\} \\ &= \sum_S D(P(Y|S)||Q|S) - D(P_Y||Q). \end{aligned} \tag{17}$$

Thus, we can design the distribution $Q = Q(Y)$ relying on the dimming level γ, and obtain the following upper bound on the mutual information,

$$I_{UB}(X;Y) = \min \left\{ \frac{H(S)}{L}, \frac{\min_Q \sum_S D(P_{Y|S}||Q|S)}{L} \right\}. \tag{18}$$

When the dimming level is denoted by γ, we can design $Q(Y)$ as follows:

$$Q(Y) = (1-\gamma)\mathcal{N}(-\mu, \sigma_0^2) + \gamma \mathcal{N}(\mu, \sigma_1^2), \tag{19}$$

since the received signal is a mixture of two Gaussian distributions, as discussed in Section II. For the unary 4 code, we have $Q(Y) = \frac{2}{5}\mathcal{N}(-\mu, \sigma_0^2) + \frac{3}{5}\mathcal{N}(\mu, \sigma_1^2)$ corresponding to bits one and zero respectively; and 2μ is the mean gap of bit 1 and bit 0.

The upper bound is shown in Figure 13 for the transmit voltages of 23.5V, 24.5V, and 25.5V.

B. LOWER BOUND

The achievable transmission rate of Equation (15) may also be formulated as follows:

$$I(S;Y) = H(S) - H(S|Y). \tag{20}$$

In this work, we assume a uniform probability of the symbols S over the set $\{1,\ 2,\ 3,\ 4\}$. Hence, the entropy of the transmitted symbols $H(S)$ is given by $H(S) = 2$. Furthermore,

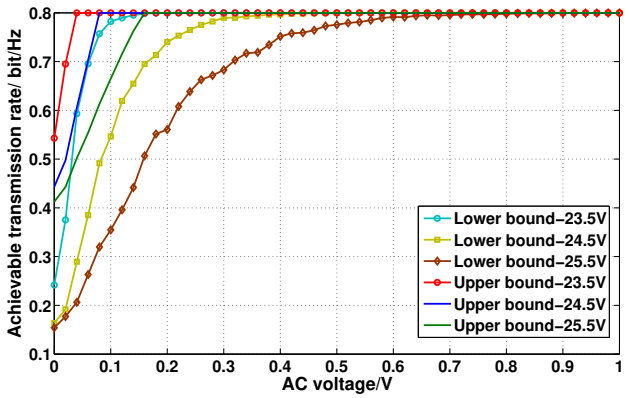

FIGURE 13. The lower bound on the achievable transmission rate for the 4-level unary codes.

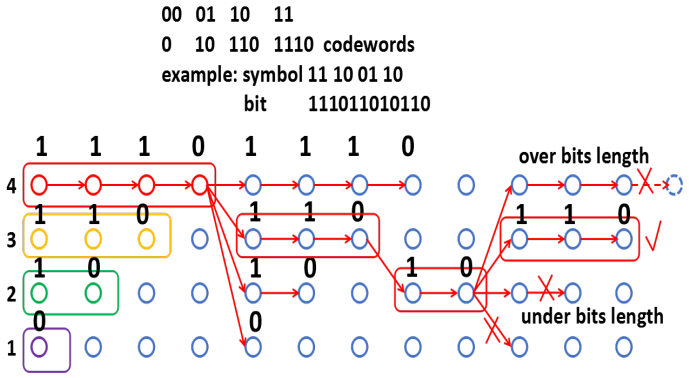

FIGURE 14. Viterbi decoding based on trellis as bits and symbol lengths known at receiver side.

according to Fano's inequality, we have the following upper bound on the conditional information [22],

$$H(S|Y) \leq H(p_e) + p_e \log(|S| - 1), \quad (21)$$

where p_e is the error probability of the received codewords $\{0,\ 10,\ 110,\ 1110\}$. Recall that bit 1 and bit 0 have the opposite mean values of μ and $-\mu$, as well as different variances of σ_1^2 and σ_0^2, respectively. Thus, assuming that $\hat{x}$ denotes the detected bit, let $p_0 \triangleq P(\hat{x} = 1|x = 0)$ and $p_1 \triangleq P(\hat{x} = 0|x = 1)$ denote the conditional detection error probability of bits zero and one, respectively. Let e denote the erroneously detected bits. Next, we calculate the error probability of all 4-level unary codewords as follows:

$$P(e|0) = p_0, \quad (22)$$
$$P(e|10) = 1 - (1 - p_0)(1 - p_1), \quad (23)$$
$$P(e|110) = 1 - (1 - p_0)(1 - p_1)^2, \quad (24)$$
$$P(e|1110) = 1 - (1 - p_0)(1 - p_1)^3. \quad (25)$$

Then, an upper bound on the detection error probability of Equation (21) can be calculated as follows,

$$P_e = \frac{1}{4}[P(e|0) + P(e|10) + P(e|110) + P(e|1110)]. \quad (26)$$

The lower bound on the mutual information obtained using the Fano inequality of Equation (21) is shown in Figure 13. For a sufficiently high AC voltage, the lower bound approaches 0.8, which is the upper bound from Equation (18).

V. TRELLIS-BASED VITERBI DECODING

Since unary coding is a variable length coding scheme, the variable length of the codewords must be taken into account during the decoding process. In this section, we propose a Viterbi decoder for unary codes, which is benchmarked against the bit-by-bit ML detection.

Viterbi decoding is based on the assumption that any part of the optimum decoded symbols is still optimum, which is satisfied for the unary code under consideration. For the unary code associated with M symbols in our proposed decoder, the M symbols constitute the M states of the trellis. We then compute the optimal path for each received sequence in a recursive manner, as detailed below.

In the following algorithm, $\delta_t(i)$ is the maximum likelihood ratio of the state i in the symbol t. Let us define state $\Phi_t(i)$ as the previous state before state i at time instant t and $index_t(i)$ as the index of state i at time instant t.

Viterbi decoding based on a trellis assumes that the receiver side knows the lengths of the symbols and the number of bits received, which guarantees the best possible SER performance. At the receiver side we have K symbols and N bits. In this unary-M scenario, we have M symbols and M states. We compute the optimized paths at symbol index T for each state and each time. The length of the optimal path should match the number of bits and symbols.

In a nutshell, the decoding algorithm is formulated as follows:

1) Initialization. The probability of $\pi_i P(b^i|s_i)$ can be derived from the preamble, which is formulated as:

$$\delta_1(i) = \log(\pi_i P(b^i|s_i)),\ 1 \leq i \leq M; \quad (27)$$
$$\Phi_1(i) = 0; \quad (28)$$
$$index_1(i) = length(s_i); \quad (29)$$

2) For $t \geq 1$, successively perform the following updates, and record the optimal previous state for each current state. Obtain $P(b^i|s_i)$ from the preamble. Check if the length exceeds N. If so, the path can be terminated. More specifically, for $1 \leq i \leq M$, perform the following,

$$\delta_t(i) = \max_{0 \leq j \leq M} (\delta_{t-1}(j) + \log P(s_i)P(b^i|s_i)), \quad (30)$$
$$\Phi_t(i) = \arg \max_{0 \leq j \leq M} (\delta_{t-1}(j) + \log P(s_i)P(b^i|s_i)), \quad (31)$$
$$index_t(i) = index_{t-1}(i) + \Phi_t(i). \quad (32)$$

3) Find the optimal termination state and the corresponding probability given the observed sequence, and check if the bits length exceeds N. If not, try the second optimal path.

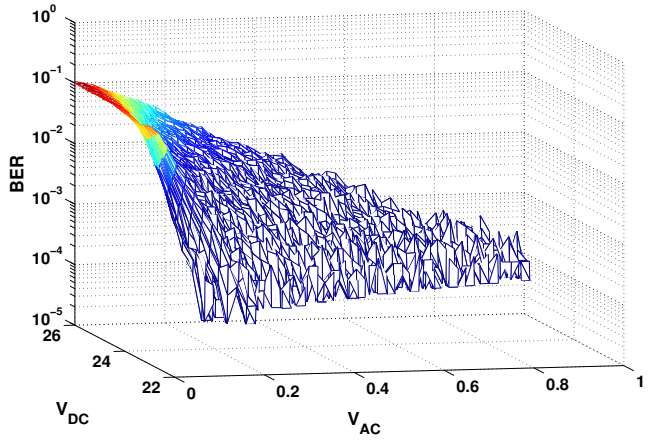

FIGURE 15. The BER for 4-level unary-coded scheme using our Viterbi decoder.

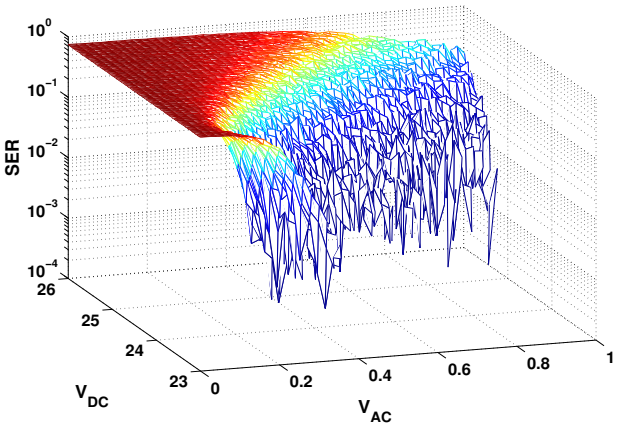

FIGURE 17. The SER performance under different DC and AC combinations for a trellis length of 100 from V_{AC} and V_{DC}.

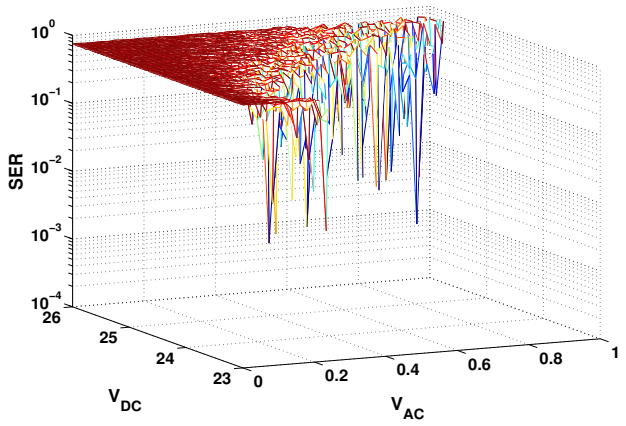

FIGURE 16. The SER for unary4 coding without trellis decoding using bit-by-bit ML decoding.

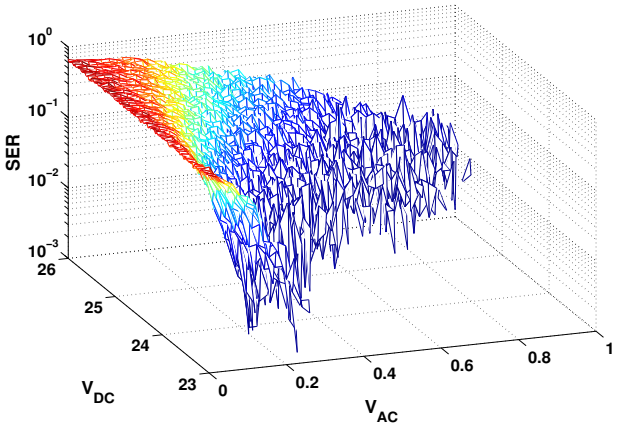

FIGURE 18. The SER performance under different DC and AC combinations at a trellis length of 10.

4) Find the optimal states or symbol sequence via the following back-tracking,

$$s_t = \Phi_{t+1}(s_{t+1}), \quad t = T, T-1, ..., 2, 1. \tag{33}$$

The BER of the Viterbi decoder is shown in Figure 15, which is significantly lower than that of the bit-by-bit ML detector shown in Figure 16. However, the SER performance of per-bit ML detection can be as high as 75% under unary-4 coding owing to the avalanche-like error propagation.

There is a trade-off between the trellis lengths N and SER. Explicitly, if the trellis is too long, the SER may become higher than that of a short trellis.

In Figure17 and 18, the SER based on a trellis length of 100 and 10 are given, respectively. It can be seen that for a trellis length of 10, the SER is lower than for 100.

VI. CONCLUSIONS

In this paper, we have investigated the signal characteristics of VLC under strong ambient light conditions which cause saturation and decreases the output signals amplitude as the DC component increases. Based on the signal characteristics, we have investigated the achievable transmission rate and link budget. Moreover, we have invoked a 4-level unary coding for dimming control, and derived the upper as well as lower bounds on the transmission rate. Finally, we proposed trellis-based Viterbi decoding for 4-level unary coding, which outperforms bit-by-bit ML detection.

REFERENCES

[1] S. Dimitrov, and H. Haas. Principles of LED Light Communications: Towards Networked Li-Fi. Cambridge University Press, 2015.
[2] H. Haas, Wireless Data from Every Light Bulb, TED Website, Aug. 2011.
[3] IEEE Std 802.15.7.C2011, IEEE Standard for Local and Metropolitan Area Networks, Part 15.7: Short-range Wireless Optical Communication Using Visible Light, 2011.
[4] D. Tsonev, H. Chun, S. Rajbhandari, J. McKendry, S. Videv, E. Gu, M. Haji, S. Watson, A. Kelly, G. Faulkner, M. Dawson, H. Haas, and D. O'Brien, "A 3-Gb/s single-LED OFDM-based wireless VLC link using a Gallium Nitride uLED," IEEE Photonics Technology Letters, vol. 26, no. 7, pp.637-640, Apr. 1 2014.
[5] G. Cossu, A. M. Khalid, P. Choudhury, R. Corsini and E. Ciaramella, "3.4

Gbit/s visible optical wireless transmission based on RGB LED," Optics Express, vol. 20, no. 26, pp. 501-506, 2012.
[6] J. Armstrong, "OFDM for optical communications," Journal of Lightwave Technology, vol. 27, no. 3, pp. 189-204, Feb. 2009.
[7] Q. Wang, Z. Wang, L. Dai, and J. Quan, "Dimmable visible light communications based on multilayer ACO-OFDM," IEEE Photonics Journal, vol. 8, no. 3, p. 7905011, Jun. 2016.
[8] B. Bai, Z. Xu, and Y. Fan, "Joint LED dimming and high capacity visible light communication by overlapping PPM," in Wireless and Optical Communications Conference (WOCC), pp. 1-5, May, 2010.
[9] S. Lou, C. Gong, N. Wu, and Z. Xu, "Joint dimming and communication design for visible light communication," IEEE Communications Letters, vol. 21, no. 5, pp. 104-1046, May 2017.
[10] T. Borogovac, M. B. Rahaim, M. Tuganbayeva, and T. D. C. Little, ""Light-off" visible light communication," in Workshop on Optical Wirless Commnication, GLOBECOM, Dec. 5-9, 2011.
[11] P. M. Butala, J. C. Chau, and T. D. C. Little, "Metameric modulation for diffuse visible light communications with constant ambient lighting," in Proc. of International Workshop on Optical Wireless Communications (IWOW), Oct. 22, 2012.
[12] H. Shen, Y. Deng, W. Xu and C. Zhao, "Rate Maximization for Downlink Multiuser Visible Light Communications," IEEE Access, vol. 4, pp. 6567-6573, 2016.
[13] F. Jin, X. Li, R. Zhang, C. Dong and L. Hanzo, "Resource Allocation Under Delay-Guarantee Constraints for Visible-Light Communication," IEEE Access, vol. 4, pp. 7301-7312, 2016.
[14] C. Gong, S. Li, Q. Gao, and Z. Xu, "Power and rate optimization for visible light communication sysytem with lighting constraints," IEEE Transactions on Signal Processing, vol. 63, no. 16, pp. 4245-4256, Aug. 2015.
[15] K. Ying, H. Qian, R. J. Baxley, and S. Yao, "Joint optimization of precoder and equalizer in MIMO VLC systems," IEEE Journal of Selected Areas in Communications, vol. 33, no. 9, pp. 1949-1958, Sept. 2015.
[16] Q. Gao, C. Gong, and Z. Xu, "Joint transceiver and offset design for visible light communications with input-dependent noise," IEEE Transactions on Wireless Communications, vol. 16, no. 5, pp. 2736-2747, May 2017.
[17] S. Yao, X. Zhang, H. Qian and X. Luo, "Joint Dimming and Data Transmission Optimization for Multi-User Visible Light Communication System," IEEE Access, vol. 5, pp. 5455-5462, 2017.
[18] T. Borogovac, M. B. Rahaim, M. Tuganbayeva, and T. D. C. Little, ""Light-off" Visible Light Communication," in Workshop on Optical Wirless Commnication, GLOBECOM, 2011.
[19] Z. Tian, K. Wright, and X. Zhou, "The darklight rises: visible light communication in the dark: Demo", Proceedings of the 22nd Annual International Conference on Mobile Computing and Networking. ACM, pp. 495-496, Oct. 2016.
[20] B. G. GuzmÃąn, V. P. G. JimÃl'nez, M. C. Aguayo-Torres, H. Haas, and L. Hanzo,"Downlink Performance of Optical OFDM in Outdoor Visible Light Communication," IEEE Access, Vol. 6, pp. 76854-76866, Nov. 22, 2018.
[21] Z. Babar, M. A. M. Izhar, H. V. Nguyen, P. Botsinis, D. Alanis, D. Chandra, S. X. Ng, R. G. Maunder, and L. Hanzo, "Unary-Coded Dimming Control Improves ON-OFF Keying Visible Light Communication," IEEE Transactions on Communications, vol. 66, no. 1, pp. 255 - 264, Jan. 2018.
[22] T. M. Cover and J. A. Thomas, Elements of Information Theory, John Wiley & Sons, 2012.

XIAONA LIU received the B.S. degree in information engineering from the South China University of Technology, Guangdong, China, in 2013. She received Ph.D. in information and communication engineering from the University of Science and Technology of China in 2018. She is currently working in the Chinese University of Hongkong, Shenzhen (CUHKSZ). Her research interests include signal detection in visible light communication (VLC), scattering optical wireless communication, information theory in VLC, weak light communication, and machine learning and neural network in positioning.

CHEN GONG received the B.S. degree in electrical engineering and mathematics (minor) from Shanghai Jiaotong University, Shanghai, China, in 2005, the M.S. degree in electrical engineering from Tsinghua University, Beijing, China, in 2008, and the Ph.D. degree from Columbia University, New York City, NY, USA, in 2012. He was a Senior Systems Engineer with the Qualcomm Research, San Diego, CA, USA, from 2012 to 2013. He is currently a Faculty Member with the University of Science and Technology of China. His research interests include wireless communications, optical wireless communications, and signal processing. He was selected by the Young 1000 Talent Program of China Government in 2014.

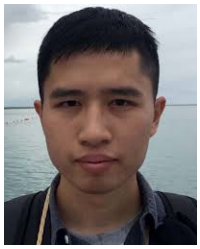

DIFAN ZOU received the B.S. degree in applied physics from the University of Science and Technology of China in 2014, and the M.S. degree in electrical engineering in the University of Science and Technology of China in 2017. He is currently pursuing the Ph.D. in UCLA, USA.

ZUNAIRA BABAR received the B.Eng. degree in electrical engineering from the National University of Science & Technology, Islamabad, Pakistan, in 2008, as well as the M.Sc. (Hons.) degree and the Ph.D. degree in wireless communications from the University of Southampton, U.K., in 2011 and 2015, respectively. Her research interests include quantum error correction codes, channel coding, coded modulation, iterative detection, and cooperative communications.

ZHENGYUAN XU received the B.S. and M.S. degrees from Tsinghua University, Beijing, China, and the Ph.D. degree from the Stevens Institute of Technology, Hoboken, NJ, USA. From 1999 to 2010, he was with the University of California at Riverside, Riverside, CA, USA, where he became a Full Professor with tenure and also a Founding Director of the UC-Light Center. In 2010, he was selected by the Thousand Talents Program of China and appointed as a Professor with Tsinghua University. Since 2013, he has been a Professor with the Department of Electronic Engineering and Information Science, School of Information Science and Technology, University of Science and Technology of China, Hefei, China. He is the Founding Director of the Wireless-Optical Communications Key Laboratory, Chinese Academy of Sciences, and a Chief Scientist with the National Key Basic Research Program of China. He has authored more than 200 journal and conference papers. He has delivered tutorials, keynote speeches, and invited talks on optical wireless communications in various international conferences. His research interests include wireless communication and networking, wireless big data, optical wireless communications, geolocation, and signal processing. He was an Associate Editor and a Guest Editor for different IEEE journals, and a Founding Co-Chair of the IEEE GLOBECOM Workshop on Optical Wireless Communications.

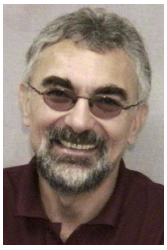

LAJOS HANZO received the First-classMaster degree in electronics in 1976, the Ph.D. degree in 1983, and the Doctor Honoris Causa degree from the Technical University of Budapest in 2009. During the 37 years of career in telecommunications, he has held various research and academic positions in Hungary, Germany, and the U.K. Since 1986, he has been with the School of Electronics and Computer Science, University of Southampton, U.K., where he holds the Chair in Telecommunications. He has successfully supervised over 119 Ph.D. students, has co-authored 20 John Wiley/IEEE Press books in mobile radio communications totalling in excess of 10 000 pages, and authored over 1800 research entries at the IEEE Xplore. He has over 44 000 citations. He is a fellow of the Future Institute of Engineering and Technology, and the European Association for Signal Processing. He has acted as the TPC and General Chair of the IEEE conferences, presented keynote lectures, and received a number of distinctions. He is directing the an academic research team, working on a range of research projects in the field of wireless multimedia communications sponsored by the industry, the Engineering and Physical Sciences Research Council, U.K., the European Research Council's Advanced Fellow Grant, and the Royal Society's Wolfson Research Merit Award. He is an enthusiastic supporter of industrial and academic liaison, and offers a range of industrial courses. He is also a Governor of the IEEE Vehicular Technology Society. From 2008 to 2012, he was the Editor-in-Chief of the IEEE Press and a Chair Professor with Tsinghua University, Beijing. His research is funded by the European Research Council's Senior Research Fellow Grant.